

Mesososcopic Modeling for Continua with Pores: Dynamic Void Growth in Viscoplastic Metals

Kerstin Weinberg, Thomas Böhme

January 22, 2007

1 Introduction

In today's engineering the question of reliability and failure of the applied materials is of raising importance. As a consequence of severe thermal and mechanical loading even initially homogeneous materials start to develop a certain microstructure, e.g., distortions of the metal lattice, micro-cracks and pores. So it is reasonable to ask for a physical measure of these microscopic changes in order to avoid catastrophic failure. Such microstructural evolution can efficiently be analyzed by means of the mesoscopic theory developed by Muschik et. al., [MPE01], which represents a general approach for the description of complex internal structured materials within the continuum mechanical framework.

In [WB06] the authors presented a mesoscopic concept for the theoretical description of elastic bubble oscillation in soft biological tissue. This was done regarding the interest in the physical phenomena occurring during the ultrasonic treatment of kidney stones. In the present paper we focus on *dissipative* materials in which the internal structure is characterized by a micro-void distribution. Such material defects were observed in many technical components. Examples are (cf. [Bel02, TI77, XP05]):

(1) *Void growth in spallation planes*, cf., Figure 1(a). Voids represent the initial stage of *dynamic fracture* observable in the surface area of ductile metals during high pressure impulses. The extremely high tension within the material lead to void nucleation at internal defects, such as impurities or grain boundaries. This damage proceeds and results in fast void expansion leading to void sheets and final failure by void coalescence.

(2) *The formation and growth of KIRKENDALL voids* within the interface of solder and substrate in microelectronic packages, cf., Figure 1(b). Here the Si-chips are typically fixed

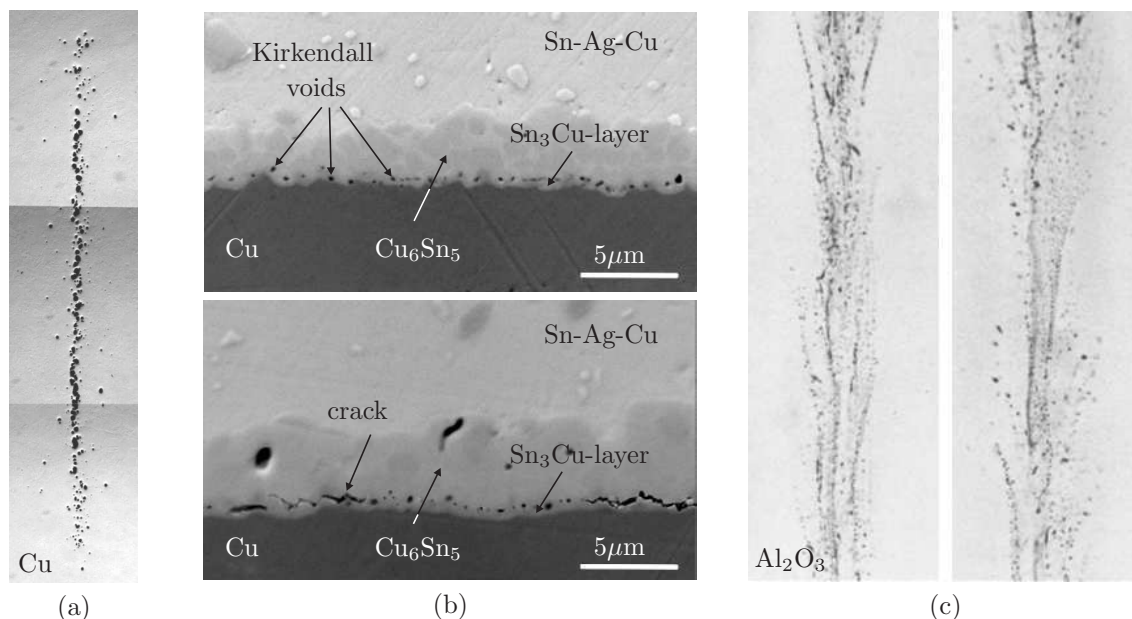


Figure 1: Technical relevant examples showing void distributions: (a) Void distribution in the spallation layer of copper, [Bel02]. (b) KIRKENDALL voids between solder and substrate, [XP05]. (c) Micro-voids in sapphire filaments, [TI77].

at the substrate (e.g., polished Cu) by means of solder materials (e.g., Sn-Ag-Cu) in which Intermetallic Compounds (e.g., Cu_3Sn or Cu_6Sn_5) are formed near the solder-substrate interface, Figure 1(b). The so-called KIRKENDALL voids appear between the Cu substrate and the thin Cu_3Sn layer due to the migration of Cu atoms from Cu_3Sn into Cu_6Sn_5 , which is much faster than the Sn-diffusion from Cu_6Sn_5 towards Cu_3Sn . This unbalanced Cu-Sn interdiffusion generates atomic vacancies at the lattice sites which coalesce to the KIRKENDALL voids, cf. [XP05].

(3) *Micro-void formation in mono-crystal growing.* Here voids grow during the crystallization process, i.e., while a crystal is pulled from the melt bubbles of dissolved or surrounding gases may be included. The resulting void distribution depends on the growth conditions and it considerably affects the material behavior of the mono-crystal. Figure 1(c) illustrates a void-distribution in mono-crystalline sapphire - a widely used material in high-technology applications (e.g., in high-power lasers).

Although the origins of the voids in the presented examples are completely different — the resulting microstructure of the materials is similar. The materials contain a certain fraction of voids separated by matrix material. Moreover, the void radii differ within a certain range and may grow in the case of external loading. Therefore, we model here the voids by an ensemble of spherical inclusion in a matrix material. This model, which will be described in

detail in the next section, enables us to link the mechanisms of void expansion and global softening of the material to parameters which describe the micro-mechanical mechanisms in a porous solid. After a brief retrospective on the mesoscopic concept we turn the attention in Section 3 to a constitutive model for void expansion in a material which is assumed to behave visco-plastically. In Section 4 we study different void ensembles and present numerical results. We finish with a short summary and an outlook in Section 5.

2 Model of a Porous Metal

In typical technical and natural materials the pores and cavities are small compared to the size of the structure. Let their distribution within a volume element dV be described by the void volume fraction, $f_V(\mathbf{x}, t) \in \mathbb{R}$, representing the void volume per current volume at the position \mathbf{x} and time t in the material. Here we presume the initial void volume fraction $f_{V0} \equiv f_V(\mathbf{x}, t = 0)$ to be small. For engineering metals it is in the range of $f_{V0} = 10^{-4} \dots 10^{-2}$, cf. [Tve90], caused, e.g., by defects in the crystal lattice or by (empty) inclusions along grain boundaries. Through straining of the material element the pores and cavities may grow but, typically, metals fail by ductile fracture at about $f_V = 0.1 \dots 0.3$ [Tve90].

2.1 The Spherical Shell Model

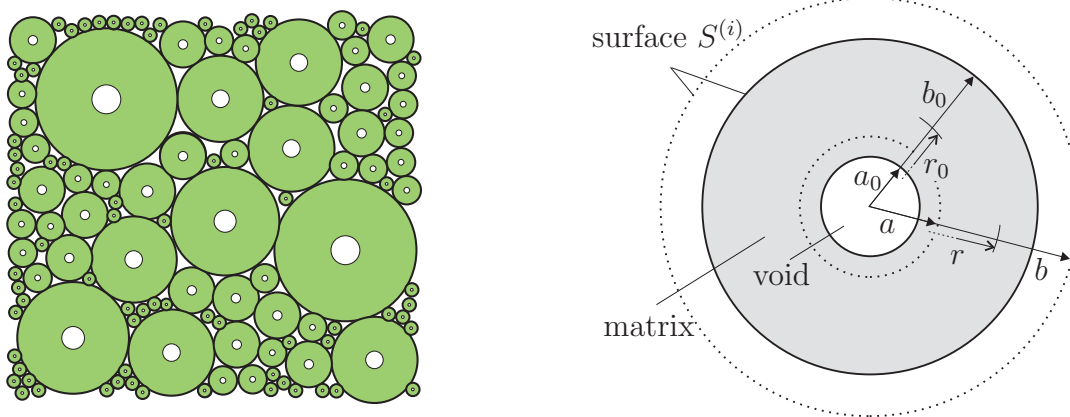


Figure 2: *Left:* Porous composite consisting of spherical shells. *Right:* Spherical shell model of a single void before and after (dashed lines) the deformation.

In order to analyze the growth of pores and cavities (voids) in a deforming solid we imagine the material to be a conglomerate of initially very small spherical voids each surrounded

by a sphere of matrix material, see Figure 2 (left). In other words, each void i with radius $a \equiv a^{(i)}(\mathbf{x}, t)$ and volume $V_{\text{void}}^{(i)} = 4\pi/3 a^3$ is at every instance completely embedded in a **spherical shell**. We exclude here the process of coalescence and it holds for each spherical shell with radius $b \equiv b^{(i)}(\mathbf{x}, t)$ and volume $V_{\text{shell}}^{(i)} = 4\pi/3 b^3$,

$$\sum_i V_{\text{shell}}^{(i)} = V - V_{\text{rem}} \quad \text{and} \quad V_{\text{void}}^{(i)}/V_{\text{shell}}^{(i)} = \frac{a^3}{b^3} = f_V^{(i)}. \quad (1)$$

Here V denotes the total volume and V_{rem} is the volume remaining between the spheres.

The porous material is now modelled as an assemblage of such spherical shells with a certain given initial void volume fraction and an initial size distribution. During the process of deformation the spherical shells may grow (in different ways) but retain their shapes whereas the matrix material follows classical material laws. As the remaining volume between the spheres can be made infinitesimally small, we assume, for simplicity, $V_{\text{rem}} \rightarrow 0$. Then, the deformation energy of the composite body will in the limit approach the sum of deformation energies of all spherical shells.

Figure 2 (right) illustrates *one* spherical shell in its undeformed and deformed state. An arbitrary material sphere surrounding the void and deforming with the body has initial and current radii $r_0 \in [a_0, b_0]$ and $r \equiv r(t) \in [a, b]$, respectively. Presuming a volume preserving deformation, i.e.,

$$\frac{d}{dt} \frac{4\pi}{3} (r^3 - a^3) = 0 \quad \Rightarrow \quad r_0^3 - a_0^3 = r^3 - a^3, \quad (2)$$

gives the current radius as $r = (r_0^3 - a_0^3 + a^3)^{1/3}$. As a consequence, the current outer radius of an incompressible shell is uniquely determined by $b(a) = (b_0^3 - a_0^3 + a^3)^{1/3}$, and all subsequent equations depending on radius b can be expressed in terms of void radius a and the initial geometry. Moreover, eq. (2) defines the deformation velocity field over the current configuration. In particular, the radial component of the spatial velocity reads

$$v_r = \frac{dr}{dt} = \frac{a^2}{r^2} \dot{a}, \quad (3)$$

where the rate of void radius, $\dot{a} \equiv \dot{a}(a, t) = \frac{da}{dt}$, identifies the velocity of void expansion or compression, here simply denoted as **void velocity**.

2.2 Mesoscopic Variables and Void Distribution Function

The temporal change of a mass-specific quantity $\psi(\mathbf{x}, t)$ in a body with domain $\Omega(t)$ can be invoked by production Π^ψ and supply Σ^ψ within the body and by a flux \mathbf{J}^ψ over the boundaries. Thus, the generic *balance equation* reads in local form (cf. [Mül01])

$$\frac{\partial \rho \psi}{\partial t} + \nabla \cdot (\mathbf{v} \rho \psi + \mathbf{J}^\psi) = \Pi^\psi + \Sigma^\psi, \quad (4)$$

where ρ is the current mass density and $\mathbf{v}(\mathbf{x}, t)$ denotes the material velocity. The specific balances of mass, momentum, total and internal energy, etc. follow directly by inserting the according expressions for ψ , \mathbf{J}^ψ , Π^ψ and Σ^ψ .

The fundamental idea of the mesoscopic concept is to extend the classical space-time domain of these quantities by a set of additional parameters, the mesoscopic variables \mathbf{m} . The fields appearing in the classical balances equations are now defined on a so-called mesoscopic space $\{\mathbf{x}, t, \mathbf{m}\}$. In our case of a porous metal the mesoscopic variables are simply the void radii $a(t)$ of the different spherical shells¹ in a volume element at position \mathbf{x} .

Additionally, a statistical function is introduced. This **mesoscopic distribution function** $\tilde{d}(\mathbf{m}, \mathbf{x}, t) \in \mathbb{R}$ describes the distribution of the mesoscopic variables: in the volume element associated with (\mathbf{x}, t) the value of the mesoscopic variables \mathbf{m} has fraction \tilde{d} of all particles. Now the fields of mass density, momentum, total energy etc. can be defined on the mesoscopic space. For distinguishing these fields from the usual, macroscopic ones and to omit the arguments in the remaining of the text, we add a tilde to symbol, i.e., $\tilde{\rho} \equiv \tilde{\rho}(\mathbf{m}, \mathbf{x}, t)$, $\tilde{\mathbf{v}} \equiv \tilde{\mathbf{v}}(\mathbf{m}, \mathbf{x}, t)$, $\tilde{e} \equiv \tilde{e}(\mathbf{m}, \mathbf{x}, t)$ and so on.

From a mathematical point of view, the mesoscopic balance equations differ from the macroscopic ones only in their domain which is enlarged by the mesoscopic variables. Therefore, derivatives with respect to these variables now appear in the balances. Thus, the generic *mesoscopic balance equation* reads in local form (cf. [MPE04])

$$\frac{\partial}{\partial t} \tilde{\rho} \tilde{\psi} + \nabla_{\mathbf{x}} \cdot [\tilde{\mathbf{v}} \tilde{\rho} \tilde{\psi} - \tilde{\mathbf{J}}^{\psi, \mathbf{x}}] + \nabla_{\mathbf{m}} \cdot [\tilde{\mathbf{u}} \tilde{\rho} \tilde{\psi} - \tilde{\mathbf{J}}^{\psi, \mathbf{m}}] = \tilde{\Pi}^{\tilde{\psi}} + \tilde{\Sigma}^{\tilde{\psi}}. \quad (5)$$

The mesoscopic change velocity $\tilde{\mathbf{u}} \equiv \tilde{\mathbf{u}}(\mathbf{m}, \mathbf{x}, t)$ is the analog to the material velocity $\tilde{\mathbf{v}}$; in our model it is the void velocity \dot{a} defined in eq (3). Moreover, derivative $\nabla_{\mathbf{m}}$ stands here for $\partial/\partial a$. Mesoscopic balances of mass, momentum and energy can now be formulated.

¹The sole use of the scalar mesoscopic variable a presumes a dependence between the radii $a(t)$ and $b(t)$ within the spherical shell ensemble as described above. A more general case could be found introducing a vectorial mesoscopic variable $\mathbf{m} = (a, b)$.

The mesoscopic concept does not introduce new balance for the additional fields through these are included in the mesoscopic space. However, the mesoscopic distribution function \tilde{d} and the mesoscopic change velocity \dot{a} require additional equations. To specify the mesoscopic distribution function for the porous material under consideration here let $\tilde{N}_V = \tilde{N}_V(a, \mathbf{x}, t)$ be the number of shells with voids of radius a in the volume element at $\{\mathbf{x}, t\}$. We presume that all voids have a nucleation size a_0 and that the void radius is bounded by half of the characteristic length of the volume element, $l_{VE} = \sqrt[3]{dV}$. Then, the total number of voids per unit volume results as

$$N_V(\mathbf{x}, t) = \int_{a_0}^{l_{VE}/2} \tilde{N}_V da, \quad (6)$$

and we define the mesoscopic **void distribution function** by

$$\tilde{d} \equiv d(a, \mathbf{x}, t) = \frac{\tilde{N}_V}{N_V(\mathbf{x}, t)} \quad \text{with normalization} \quad \int_{a_0}^{l_{VE}/2} \tilde{d} da = 1. \quad (7)$$

In order to obtain an evolution equation for the void distribution function we start from eq. (5) and formulate the balance of the mesoscopic void number density

$$\frac{\partial \tilde{N}_V}{\partial t} + \nabla_x \cdot (\tilde{N}_V \tilde{\mathbf{v}}) + \frac{\partial}{\partial a} (\tilde{N}_V \dot{a}) = \tilde{\Pi} \tilde{N}_V, \quad (8)$$

where symbol $\tilde{\Pi} \tilde{N}_V$ denotes a production term referring to void nucleation and/or coalescence. Because all voids are embedded in the matrix of the solid (and do not move independently), the mesoscopic velocity $\tilde{\mathbf{v}}$ is identical for all voids and equals the macroscopic velocity of the volume element, $\tilde{\mathbf{v}} = \mathbf{v}(\mathbf{x}, t)$. Multiplying eq. (8) with $1/N_V$ and applying eq. (7) results after a minor calculation in

$$\frac{\partial \tilde{d}}{\partial t} + \nabla_x \cdot (\tilde{d} \mathbf{v}) + \frac{\partial}{\partial a} (\tilde{d} \dot{a}) = \tilde{\Pi} \tilde{N}_P + \frac{\tilde{d}}{N_P} \left(\frac{\partial N_P}{\partial t} + \mathbf{v} \cdot \nabla_x N_P \right). \quad (9)$$

The right hand side of (9) represents two different but not independent production terms, for a discussion see [WB06]. Here we do neither consider void nucleation nor coalescence and these terms vanish. Thus, eq. (9) becomes a conservation law and the *balance of the void distribution function* reads:

$$\frac{\partial \tilde{d}}{\partial t} + \nabla_x \cdot (\tilde{d} \mathbf{v}) + \frac{\partial}{\partial a} (\tilde{d} \dot{a}) = 0. \quad (10)$$

By means of eq. (10) the evolution of voids in a general material is predictable. For application to the specific materials we envision here, the constitutive equation for the void velocity within the ensemble, $\dot{a}(a, \mathbf{x}, t)$, remains to be specified.

3 Constitutive Model

In what follows we want to consider the deformation process of a volume element dV containing an ensemble of spherical shells. We postulate the existence of a **free energy** function $A(\mathbf{x}, t)$ as a weighted sum of free energy contributions of *all* spherical shells. The energy required to deform *one* shell, \tilde{A} , is a sum of energy contributions accompanying shell deformation and void expansion.

Exposing the spherical shell ensemble to externally applied forces, e.g., a **tension field** $p(t)$, generally invokes an inhomogeneous stress field. In this model we assume an *averaged* stress field of the form $\boldsymbol{\sigma}(a, \mathbf{x}, t) \doteq \boldsymbol{\sigma}$, i.e., all spherical shells “feel” the same loading². Moreover, we assume the power of the external forces acting on *one* spherical shell $\tilde{P} \equiv P(a, \mathbf{x}, t)$ to be completely compensated by the rate of free energy,

$$\tilde{P} = p(t) \cdot \frac{d\tilde{V}_{\text{shell}}}{dt} \stackrel{!}{=} \frac{d\tilde{A}}{dt}. \quad (11)$$

With a specified right hand side and with initial values a_0 and b_0 eq. (11) represents a differential equation for the void radius in one spherical shell. Solving this equation for all voids with different initial conditions yields a constitutive relation for the void velocity (3).

Let us now specify the constitutive equations for a visco-plastic material with *three* contributions to the free energy function: **(1)** energy required for plastic deformation of the matrix material \tilde{W}^p , **(2)** kinetic energy \tilde{K} of void expansion and **(3)** surface energy \tilde{S} stored in the interface between void and matrix.

Stored plastic work

Exploiting the spherical symmetry of the model and the plastic incompressibility constraint of the matrix material we can derive from the kinematics outlined in section (2) the principle stresses and strains within one shell. Correspondingly, the velocity over the current

²This assumption is established in the field of homogenization as the Reuss approximation, [GS06].

configuration (3) yields the strain rate as

$$\dot{\varepsilon}(r, t) = \frac{\partial \dot{r}}{\partial r} = -\frac{2a^2(t)}{r^3(t)} \dot{a}(t). \quad (12)$$

The absolute value of strain rate (12) defines the rate of the effective von Mises strain, $\dot{\varepsilon}^p \equiv |\dot{\varepsilon}(r, t)|$. Presuming a monotonic void growth, equation (12) can be integrated to give

$$\varepsilon^p = \left| -\frac{2}{3} \log \left(1 + \frac{a^3 - a_0^3}{r^3 - (a^3 - a_0^3)} \right) \right| = \frac{2}{3} \log \left(1 + \frac{a^3 - a_0^3}{r_0^3} \right). \quad (13)$$

Let us consider classical von Mises plasticity with power law hardening of the yield stress σ_y ,

$$\sigma_y = \sigma_0 (1 + \varepsilon^p / \varepsilon_0^p)^{1/n}, \quad (14)$$

where $n \in [1, \infty)$ denotes the hardening exponent and $\sigma_0, \varepsilon_0^p$ are the initial yield stress and a reference plastic strain, respectively. With $n = 1$ we prescribe linear isotropic hardening, whereas $n \rightarrow \infty$ enforces perfect plasticity. Additionally, one may include here a temperature dependence of the yield stress, $\sigma_0(T)$, cf. [Wei06]. The stored plastic energy density follows from the rate of plastic straining by

$$\int_0^t \sigma_y \dot{\varepsilon}^p \, d\bar{t} = \int_{\varepsilon_0^p}^{\varepsilon^p} \sigma_y \, d\varepsilon^p = \varepsilon_0^p \sigma_0(T) \frac{n}{n+1} \left[\left(1 + \frac{\varepsilon^p}{\varepsilon_0^p} \right)^{\frac{n+1}{n}} - 1 \right]. \quad (15)$$

A volume integration results in the stored plastic energy of one spherical shell:

$$\tilde{W}^p(a, b; T, n) = \int_a^b \varepsilon_0^p \sigma_0(T) \frac{n}{n+1} \left[\left(1 + \frac{\varepsilon^p}{\varepsilon_0^p} \right)^{\frac{n+1}{n}} - 1 \right] 4\pi r^2 \, dr. \quad (16)$$

Note that the result of (16) does not depend on radius r . Evaluating (16) with (13) and substituting $x := r^3/a^3$ gives

$$\tilde{W}^p(a, b; T, n) = \varepsilon_0^p \sigma_0(T) \frac{n}{n+1} \frac{4\pi a^3}{3} \int_0^{b^3/a^3} \left(1 + \frac{2}{3\varepsilon_0^p} \log \frac{x}{x - 1 + a_0^3/a^3} \right)^{\frac{n+1}{n}} dx. \quad (17)$$

By means of relation (2) the dependence of \tilde{W}^p on radius b can be eliminated and we obtain

$$\tilde{W}^p = \tilde{W}^p(a; T, n) = \varepsilon_0^p \sigma_0 \frac{n}{n+1} \frac{4\pi a_0^3}{3} g(a; n), \quad (18)$$

$$g(a; n) = \int_0^{b_0^3/a_0^3} \left\{ 1 + \frac{2}{3\varepsilon_0^p} \log \left[1 + \frac{1}{x} \left(\frac{a^3}{a_0^3} - 1 \right) \right] \right\}^{\frac{n+1}{n}} dx. \quad (19)$$

The stored energy function (18) is attributed directly to the growth of one void of radius a . The *total* stored plastic energy can be calculated by the “weighted sum” over the individual spherical shells using the mesoscopic distribution function (10). It reads:

$$W^p(\mathbf{x}, t) = \int_{a_0}^{l_{VE}/2} \tilde{d}\tilde{W}^p da. \quad (20)$$

Kinetic energy

In an analogous manner the kinetic energy of an expanding void ensemble can be determined. With the radial component of spatial velocity (3) the kinetic energy of *one* expanding void is computed to be

$$\tilde{K} = \tilde{K}(a, \dot{a}) = \int_V \frac{1}{2} \varrho \tilde{v}^2 dV = \int_a^b \frac{1}{2} \varrho_0 v_r^2 4\pi r^2 dr = 2\pi \varrho_0 a^4 \left(\frac{1}{a} - \frac{1}{b} \right) \dot{a}^2, \quad (21)$$

where ϱ_0 denotes the mass density of the matrix material which is constant because of plastic incompressibility, and $b = b(a)$. Then, analogously to eq. (20), the *total* kinetic energy of the porous ensemble follows as

$$K(\mathbf{x}, t) = \int_{a_0}^{l_{VE}/2} \tilde{d}\tilde{K} da. \quad (22)$$

Surface energy

The surface energy \tilde{S} in the interface of *one* void with radius a as well as the according *total* surface energy of the whole ensemble are determined by the relations

$$\tilde{S} := S(a) = 4\pi a^2 \gamma \quad \text{and} \quad S(\mathbf{x}, t) = \int_{a_0}^{l_{VE}/2} \tilde{d}\tilde{S} da, \quad (23)$$

where γ denotes the surface tension (in [N/m]).

External power and governing differential equation

With eq. (11) and the kinematics of Section 2 the external power of a spherical shell results in $\tilde{P} = p(t) \cdot d_t(\frac{4}{3}\pi(b_0^3 - a_0^3 + a^3))$. Consequently, we write for \tilde{P} and for the macroscopic power P consumed by the whole spherical shell ensemble:

$$\tilde{P} = p(t) \cdot 4\pi a^2 \dot{a} \quad \text{and} \quad P(\mathbf{x}, t) = \int_{a_0}^{l_{\text{VE}}/2} \tilde{d}\tilde{P} \, da. \quad (24)$$

Inserting the expressions (18), (21), (23) and (24)₁ into ansatz (11) results in

$$\begin{aligned} 0 &= \tilde{P} - \frac{d}{dt} \left(\tilde{W}^{\text{P}} + \tilde{K} + \tilde{S} \right) \\ &= p(t) \cdot a^2 \dot{a} - \varepsilon_0^p \sigma_0 \frac{n}{n+1} \frac{a_0^3}{3} \dot{g}(a; n) - 2a\gamma \dot{a} \\ &\quad - \frac{\rho_0}{2} \left[2\ddot{a}a^3 + 3\dot{a}^3 a^2 - \frac{a^3}{b} \left(2\ddot{a}a + 4\dot{a}^3 - \frac{a^3 \dot{a}^3}{b^3} \right) \right], \end{aligned} \quad (25)$$

where we abbreviate $b = (b_0^3 - a_0^3 + a^3)^{1/3}$. This ordinary differential equation can be solved (numerically) for *every* shell of radius $a(t)$ and of known initial geometry, $a_0 = a(t=0)$ and $b_0 = b(t=0)$. Once the values of void velocity \dot{a} have been found for *all* different shells the evolution of the void size distribution function can be solved by means of eq. (10).

4 Analysis of Void Ensembles

In an attempt to illustrate the capability of the constitutive model derived in the previous section we now analyze void growth for a typical metal with material data of Table 1. In

E	ν	ϱ	σ_0	ε_0^p	γ	n
69	0.33	2700	80	0.0012	5	10

Table 1: Material parameter representative of aluminum. The following units are chosen: E in [GPa], ϱ in [kg/m³], σ_0 in [MPa], and γ in [N/m].

the following we consider a volume element at fixed spatial position \mathbf{x} , i.e., $dV = dV(t)$, subjected to different loading regimes $p(t)$. Note that a positive value of $p(t)$ refers to hydrostatic tension.

4.1 Growth of equally sized voids under hydrostatic tension

We start with the special case of a void ensemble with an average radius of size \bar{a} , i.e., the initial void distribution function $\tilde{d}(t=0)$ has the form of a dirac impulse at \bar{a}_0 and remains of this shape for the expanding voids of radius $\bar{a} \geq \bar{a}_0$; for ease of reading we write $a \equiv \bar{a}$.

4.1.1 Quasistatic void growth

In case of a slow loading regime the effect of inertia can be neglected. Assuming a constant remotely applied tension \bar{p} we get from eq. (25)

$$\tilde{P} = \frac{d}{dt} (\tilde{W}^p + \tilde{S}) \quad \Rightarrow \quad \bar{p}a^2 = \frac{n\sigma_0\varepsilon_0^p a_0^3}{n+1} g'(a; n) + 2a\gamma, \quad (26)$$

where $g'(a; n)$ denotes the derivative of integral (19) w.r.t. radius a . Solving the plastic energy term of (26)₂ for the special case of perfect plasticity, i.e., $n \rightarrow \infty$, and dividing the expression by a^2 results in

$$\bar{p} = \frac{2\sigma_0}{3} (\log(a^3 - a_0^3 + b_0^3) - \log(a_0^3)) + \frac{2\gamma}{a}. \quad (27)$$

Eq. (27) defines an algebraic relation between applied tension \bar{p} and void radius a . Note that we neglect in our constitutive model any elastic void expansion. In consequence, equation (27) is actually an inequality determining a critical tension necessary to induce a void to grow plastically. This corresponds to the concept of critical **cavitation pressure** as discussed, e.g., in [Fre98, OM92, WMO06].

$$\bar{p} \geq p_y = \frac{2\sigma_0}{3} \log\left(1 + \frac{b_0^3 - a_0^3}{a^3}\right) + \frac{2\gamma}{a} \quad (\text{condition for void expansion}) \quad (28)$$

The material-specific critical cavitation pressure depends on initial and current void volume fraction. For an perfect-plastic material eq. (28) defines a high initial cavitation pressure which considerably softens immediately after the voids start to grow, see Fig. 3 (left). For a hardening material the slope is smaller, i.e., the cavitation pressure reduces slower with rising void size.

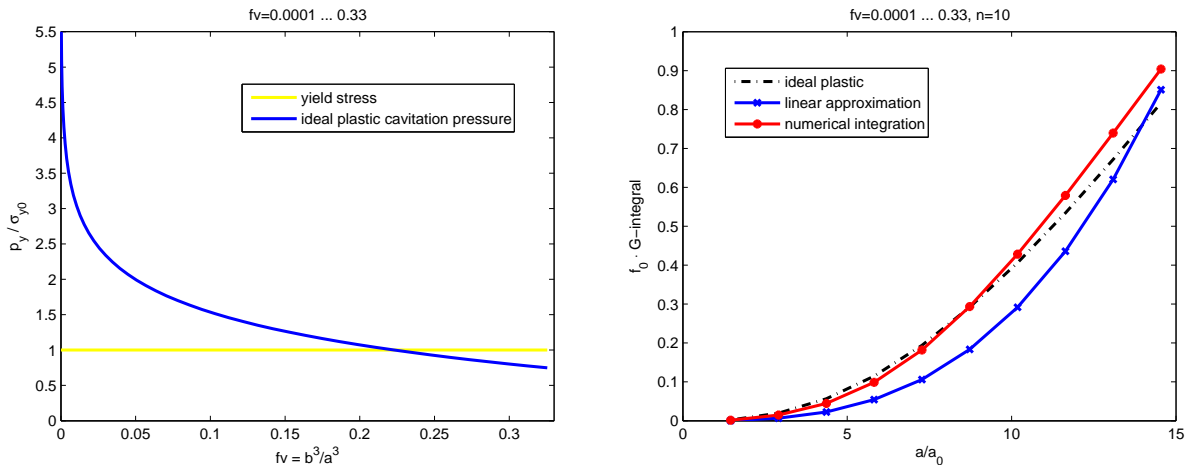


Figure 3: *Left:* Perfect plastic cavitation pressure depending on void volume fraction f_V in a quasistatic regime. *Right:* Solution and approximation of equation (19) multiplied by $(1.5\varepsilon_0^p)^{-(n+1)/n}$.

In general, an analytical expression for p_y cannot be obtained because the integral of eq. (19) is trackable by analytical means only for $n \rightarrow \infty$. If a repeated numerical solution of eq. (19) for every value of a is too cumbersome, we suggest here a simple linear approximation:

$$g(a; n) \approx h_n \left(\frac{2}{3\varepsilon_0^p} \right)^{\frac{n+1}{n}} \left(\frac{a^3}{a_0^3} - 1 \right), \quad (29)$$

where h_n is a constant depending on hardening exponent n . This constant needs to be fitted to the values of integral (19), once numerically evaluated over a range of realistic (initial and final) void volume fractions, see Figure 3 (right). We proceed here with $h_n = 2.21$ for $n = 10$ and $f_{V0} = 10^{-4}$. Note that the approximation (29) may also provide a way to fit the critical cavitation pressure to values known from experiments, if available.

Assuming from now on a hypercritical tension \bar{p} let us discuss void growth in a quasistatic regime, eq. (27). The yield stress of a material, usually in the range of some MPa, weights the first term in (27) much stronger than the surface tensions, cf. Table 1. This effect is compensated for very small void sizes by factor $1/a$. Only if the void is near vacancy size (0.5 nm – 50 nm) the surface energy contributes significantly to void growth. Otherwise, the second term in equations (27) is negligible.

In consequence, we approximate the initial cavitation pressure for void expansion in an

perfect plastic and in a hardening material ($n \in \mathbb{N}$) by

$$p_{y0} = \frac{2\sigma_0}{3} \log\left(\frac{b_0^3}{a_0^3}\right) \quad \text{and} \quad p_{y0} = \frac{n \sigma_0 \varepsilon_0^p a_0^3}{3(n+1)a^2} g'(a; n) \approx \frac{n \sigma_0 \varepsilon_0^p h_n}{n+1} \left(\frac{2}{3\varepsilon_0^p}\right)^{\frac{n+1}{n}}, \quad (30)$$

respectively.

4.1.2 Dynamic void growth in a perfect plastic material

In a next step we extend the above relations to dynamic loading regimes with a constant but hypercritical tension $\bar{p} > p_{y0}$. Integrating eq. (25) in the interval $[0, t]$ and inserting eq. (30) yields:

$$\frac{1}{3}\bar{p}(a^3 - a_0^3) = \frac{1}{3}p_{y0}(a^3 - a_0^3) + \gamma(a^2 - a_0^2) + \frac{1}{2}\varrho_0 a^4 \left(\frac{1}{a} - \frac{1}{b}\right) \dot{a}^2. \quad (31)$$

Evaluating this ODE of first order in $a(t)$ gives

$$\dot{a} = \sqrt{\frac{2}{3\varrho_0}} (\bar{p} - p_{y0} - p_\gamma)^{\frac{1}{2}} \left(\frac{1 - (a_0^3/a^3)}{1 - (a/(a^3 + b_0^3 - a_0^3)^{1/3})} \right)^{\frac{1}{2}}, \quad (32)$$

where $p_\gamma = 3\gamma(a^2 - a_0^2)/(a^3 - a_0^3)$ is the term resulting from surface energy contributions which has significance only at the beginning of the void growth process when $a \gtrsim a_0$. By the presumption of hypercritical loading is the pressure difference $\Delta p \equiv \bar{p} - p_{y0} - p_\gamma > 0$ and the second term of (32) is positive. Moreover, it is clear from equation (32) that the void velocity reduces for high density materials, whereas a small value of ϱ_0 allows the voids to grow faster. The solution of eq. (32) is displayed in Fig. 4 for $\varrho_0 = 2/3$, $\Delta p = 1$ and some realistic initial void sizes. Note that, although the applied tension \bar{p} is constant, the void velocity increases unboundedly with rising void size.

Some particular cases merit special attention:

I: $b_0 \rightarrow \infty$. This case corresponds to a void of radius a_0 in an infinite matrix as analyzed in [OM92]. Eq. (32) becomes

$$\dot{a} = \sqrt{\frac{2}{3\varrho_0}} (\bar{p} - p_{y0} - p_\gamma)^{\frac{1}{2}} \left(1 - \frac{a_0^3}{a^3}\right)^{\frac{1}{2}}, \quad (33)$$

with the third term $\in [0, 1)$. In this case (and only in this case!) the void expansion velocity is bounded.

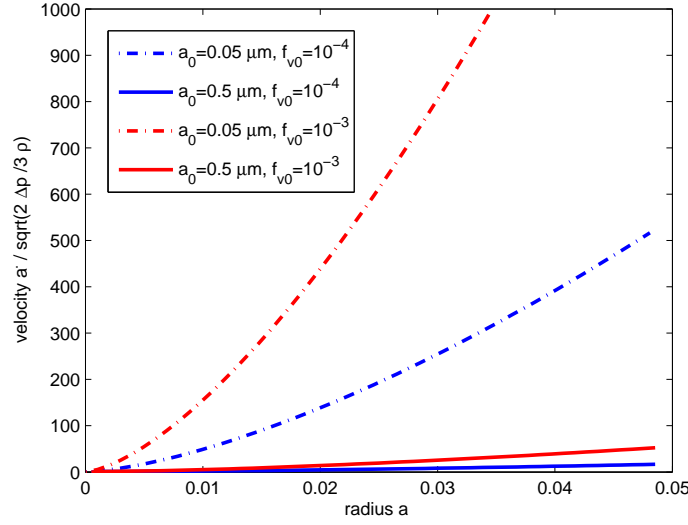


Figure 4: Velocity of void expansion as a function of radius a for different initial data.

II: $b_0 \rightarrow \infty, a_0 \rightarrow 0$. For a very small void in an *infinite* matrix the void expansion velocity is constant, namely:

$$\dot{a} = \sqrt{\frac{2}{3\rho_0}} (\bar{p} - p_{y0} - p_\gamma)^{\frac{1}{2}}. \quad (34)$$

4.1.3 Dynamic void growth in a hardening material

At next we analyze void expansion in a volume element of visco-plastic material with hardening subjected to hydrostatic tension. Evaluating eq. (25) for the void acceleration \ddot{a} gives:

$$\ddot{a} = \left\{ \frac{1}{\rho_0} \left[\bar{p}a^2 - 2a\gamma - \frac{na_0^3 \varepsilon_0^p \sigma_0}{3(n+1)} g'(a; n) \right] - \dot{a}^2 \left(\frac{3a^2}{2} - \frac{2a^3}{b} + \frac{a^6}{2b^4} \right) \right\} \times \left(a^3 - \frac{a^4}{b} \right)^{-1}.$$

In order to determine $a(t)$, $\dot{a}(t)$, and $\ddot{a}(t)$ this equation is solved numerically by recourse to a Runge-Kutta scheme with adapted time step. The derivative of integral (19) w.r.t. a , $g'(a; n)$, is computed numerically (no approximation in the sense of eq. (29) performed). The initial conditions are: $a_0 = 25\mu\text{m}$ and $f_{V0} = a_0^3/b_0^3 = 10^{-4}$.

Applying instantaneously a constant tension of 1 GPa we compute the results displayed in Figure 5. A population of voids expands, and, despite of the hardening material we observe

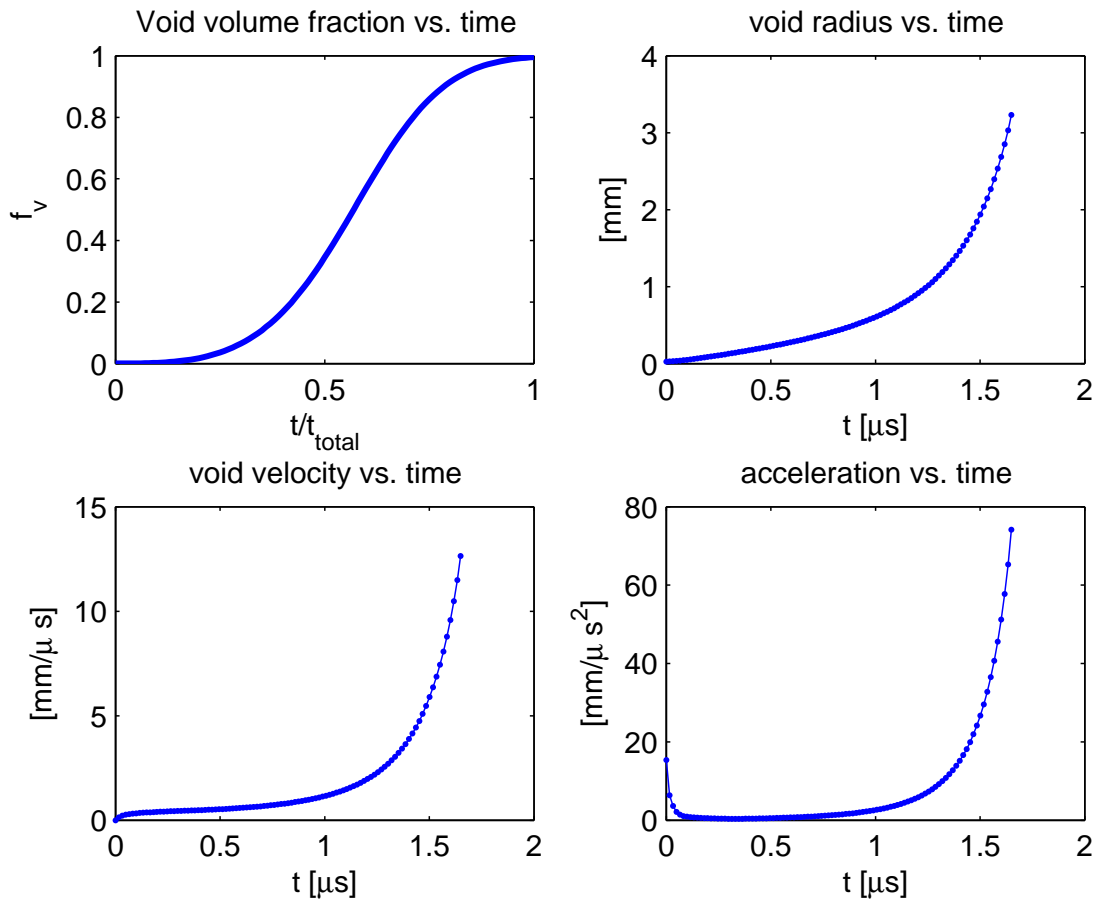


Figure 5: Void growth of an equally sized void ensemble under constant tension.

a raise of void radius, of void velocity *and* of void acceleration up to the theoretical limit of $f_V = 1$. Note that this “self-accelerating” void expansion is equivalent to a *macroscopic softening* of the composite material.

In general, the dynamic void expansion is faster the smaller the initial voids are. The surface energy retards void growth in the first stages, superposed by a significant effect of inertia. The initial void volume fraction is of small influence, but generally the void growth decelerates with lower values of f_{V0} , cf. comments in Section 4.1.2.

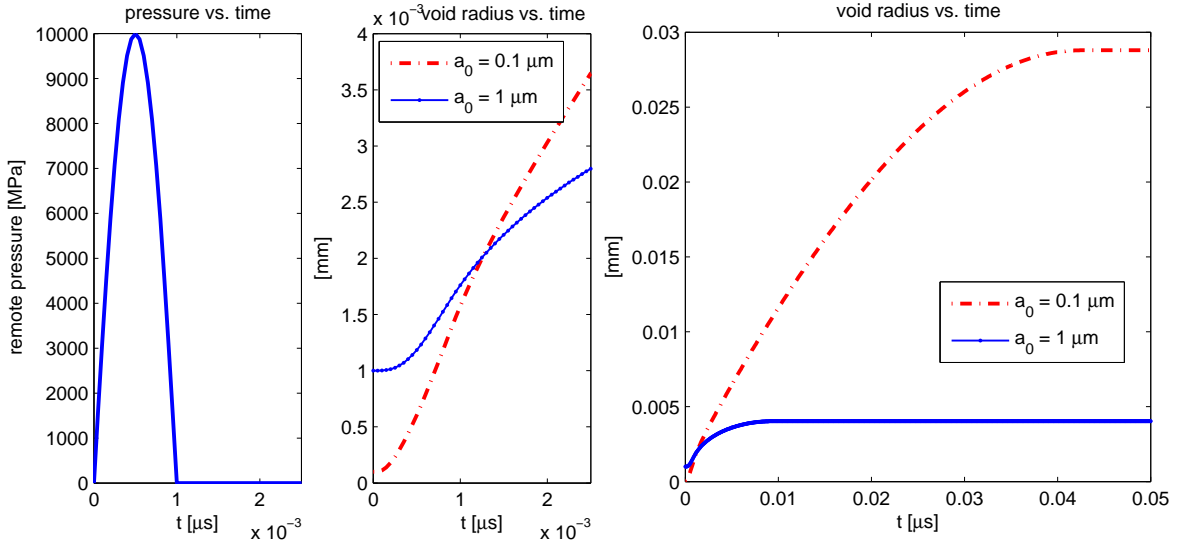


Figure 6: Inertia dominated void growth due to a pressure impulse for two different radii, short term and long term response.

4.1.4 High Pressure Impulse

Let us apply now a sinusoidal pressure impulse with an amplitude of 10 GPa within a short time interval of $t_{load} = 1$ ns. A void ensemble with $a_0 = 0.1 \mu\text{m}$ expands to $a = 1.57 \mu\text{m}$ at $t = t_{load}$. The corresponding void volume fraction rises from $f_{V0} = 10^{-4}$ to $f_V = 0.28$. Starting with the same initial void volume fraction but a smaller void size increases the void expansion. In particular we observe a dependence of the form $\dot{a}(t) \propto (\sqrt{\bar{p}}/a_0)$ for $t \in [0, t_{load}]$.

The void expansion is here clearly dominated by inertia effects. This is nicely illustrated in Figure 6 where we see that the voids continue to grow after the load impulse has passed, i.e., for $\bar{p} = 0$, $t > t_{load}$. For $a_0 = 0.1 \mu\text{m}$ the final void volume fraction reaches $f_V \rightarrow 1$. Starting with bigger voids of $a_0 = 1 \mu\text{m}$ the void velocity and size increase are smaller, $a(t = t_{load}) = 1.76 \mu\text{m}$, and the void growth converges to a final void size of $a = 4.03 \mu\text{m}$. This regime of inertia dominated void growth is of particular importance for impact and spallation problems, see, e.g. [Fre98, MM00, SCA01, WMO06].

4.2 Analysis of Void Size Distribution

After studying the principles of void growth we proceed with an ensemble of differently sized voids. Point of departure is the balance of the void distribution function (10), where we additionally assume that the body is not in motion, $\mathbf{v} = 0$.

Let the initial number of voids $\tilde{N}_V(a, t = 0)$ be given by a Gaussian distribution around an initial mean radius \bar{a}_0

$$\tilde{N}_V(a, t = 0) = \tilde{N}_V(a_0) = c_0 e^{-\frac{1}{2} \left(\frac{a_0 - \bar{a}_0}{\bar{a}_0 \epsilon_0} \right)^2} \quad (35)$$

where c_0 is a normalization factor, ϵ_0 denotes the deviation (the “width” of distribution) and an index \cdot_0 refers to the initial configuration. By means of eq. (6) the initial number of particles N_{V0} can be obtained. Introducing an integration variable $x = (a_0 - \bar{a}_0)/(\epsilon_0 \bar{a}_0 \sqrt{2})$ we get

$$N_{V0} = \int_0^\infty \tilde{N}_V(a_0) da_0 = \epsilon_0 \bar{a}_0 c_0 \sqrt{2} \int_{-1/(\epsilon_0 \sqrt{2})}^\infty e^{-x^2} dx \stackrel{(\epsilon_0 \ll 1)}{\cong} \epsilon_0 \bar{a}_0 c_0 \sqrt{2\pi} \quad (36)$$

to determine c_0 ; the approximation refers to small values of a_0 and $\epsilon_0 \ll 1$. With eq. (7) the initial void distribution function reads

$$\tilde{d}_0 = \frac{c_0}{N_{V0}} \cdot e^{-\frac{1}{2} \left(\frac{a_0 - \bar{a}_0}{\bar{a}_0 \epsilon_0} \right)^2} \approx \frac{1}{\epsilon_0 \bar{a}_0 \sqrt{2\pi}} \cdot e^{-\frac{1}{2} \left(\frac{a_0 - \bar{a}_0}{\bar{a}_0 \epsilon_0} \right)^2}. \quad (37)$$

The problem of interest is now, how does this distribution change in time. We start by discretizing the void distribution function for void radius a

$$\tilde{d}(a, t) = \lim_{\Delta a \rightarrow 0} \left(\tilde{d}(a + \Delta a, t) - \tilde{d}(a, t) \right) \quad \text{and} \quad \tilde{d}^{(i)}(t) = \tilde{d}(a^{(i)} + \Delta a, t) - \tilde{d}(a^{(i)}, t),$$

where $\tilde{d}^{(i)}$ is the distribution of voids with radii $a \in [a^{(i)}, a^{(i)} + \Delta a]$. Furthermore it holds:

$$1 = \int_{a_0}^{l_{VE}/2} \tilde{d}(a, t) da \approx \sum_{i=1}^n \tilde{d}^{(i)}. \quad (38)$$

Exemplarily we analyze a volume element with an ensemble of 5 voids ($N_V = N_{V0} = 5$), with an initial void volume fraction of $f_{V0} = 10^{-4}$ and with $a_0^{(1)} = 1\mu\text{m}$, $a_0^{(2)} = 3\mu\text{m}$, $a_0^{(3)} = 5\mu\text{m}$, $a_0^{(4)} = 7\mu\text{m}$, $a_0^{(5)} = 9\mu\text{m}$. The volume element is subjected to the sinusoidal loading impulse of Figure 6 with $p_{max} = 10$ GPa and $t_{load} = 1$ ns. With the parameter $\bar{a}_0 = 5\mu\text{m}$, $\epsilon_0 = 1/3$,

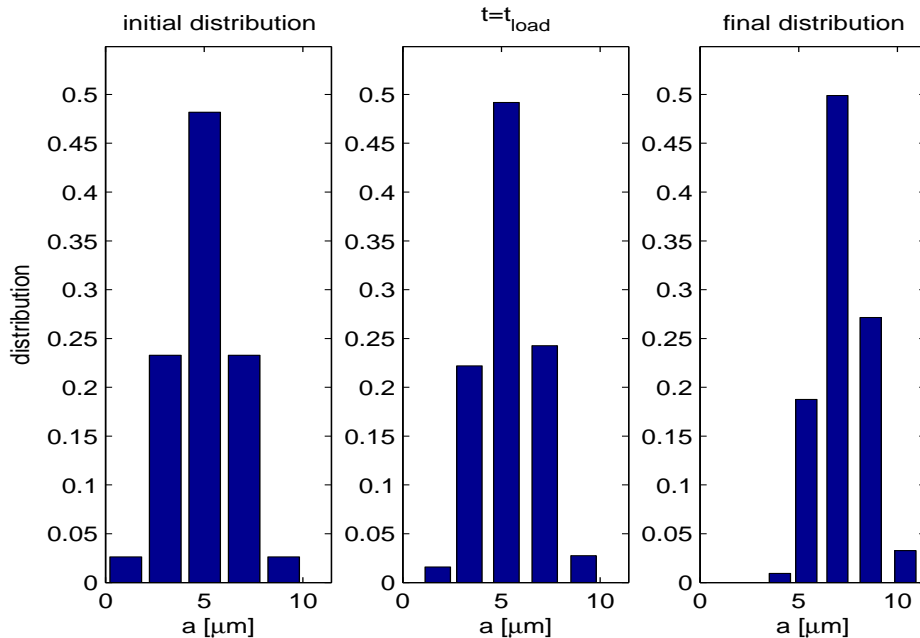


Figure 7: Initial, intermediate and final distribution in a void ensemble of 5 sizes.

$c_0 = N_{V0}/(\bar{a}_0 \epsilon_0 \sqrt{2\pi})$ and equation (37) the initial (discrete) distribution function $\tilde{d}_0^{(i)}$ is obtained, see Figure 7 (left).

As outlined in Section 4.1 we determine the mesoscopic void velocities $\dot{a}^{(i)} = \dot{a}(a^{(i)}, t)$ to solve eq. (10). Figure 7 shows the numerical solution using a Runge-Kutta scheme with time step $\Delta t \leq 10^{-11}$ s. Subjected to the loading impulse all voids grow. From the analysis of Section 4.1 we know that voids with small initial size are less inert and grow faster than their bigger companions. Consequently, the change of distribution function \tilde{d} is not symmetric. The set of small voids reduces whereas the numbers of bigger void sizes grow.

As a consequence of the inertial effects the void distribution keeps changing after the actual loading time passed. Therefore, the initial distribution, the distribution at the end of the impulse $t = t_{load}$ and the final distribution after $20\mu\text{s}$ are displayed.³ Again, the fraction of bigger voids grows. This observation is in agreement with other theories of multi-phase materials (as, e.g., Ostwald ripening or the LSW⁴ theory for liquid droplets in a gas, cf. [RV02]) where the bigger inclusions grow on cost of the smaller ones.

³Note that the width of the bars in Figure 7 has no meaning.

⁴LSW stands for the initials of the pioneers in this research: I.M. Lifshitz, V.V. Slyozov and C. Wagner.

Figure 7 already indicates that the inertial effects result is a smaller variety of void sizes, i.e., the “width” of distribution function \tilde{d} gets smaller. This trend has been supported by numerical studies of more different voids (e.g., 10 or 30 different radii). The effect may explain some of the difference between static and dynamic fracture of ductile metals. Whereas in static experiments we usually observe a cup-cone like fracture with large plastic straining and small and big (coalesced) voids, in dynamic experiments the fracture surface is more or less plain but dimpled. Voids of similar sizes grew here and set up sheets of voids resulting in fragmented surfaces, e.g. spallation planes, see Fig. 1(a).

5 Conclusions

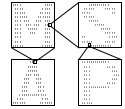
In our paper we explained a mesoscopic continuum model as well as an approach for the required material relations in order to describe the temporal development of a certain void distribution in an visco-plastic material. Moreover, in the foregoing section exemplarily results were illuminated for different loading regimes and the evolution of five different voids under a short pressure impulse was presented.

Although the physical background, the assumptions, and the interpretations of the results are completely different one can recognize similarities to the equations of so called LSW theories. So in both theories the central element is the distribution function, which characterizes the temporal development of the number of “inclusions” with a certain radius. This equation is usually ad hoc defined, whereas we derive this equation in the mesoscopic framework. Moreover, the resulting balance of the mesoscopic void distribution is more generally admitted, because it contains a production term on the right hand side and does not presume a constant volume fraction. Thus, it is possible to describe an increasing void volume as well as nucleation and coalescence of voids. However, both theories qualitatively show the same asymmetrical temporal development of the distribution function (indicated by different void velocities) but differ in the employed constitutive relation (LSW revert to the Gibbs-Thomson-equation).

Various questions and tasks are open or under current investigation, respectively. So, it is interesting to consider the behavior of voids in an elastic-plastic material. Furthermore, the question of the definition of a macroscopic damage parameter arises, characterizing, e.g., a current averaged void radius and its consequences on the classical (macroscopic) material laws. This parameter may be very similar to the damage parameter for soft tissue presented in [WB06]. Finally, investigations of (suitable) production-terms and an extension of the simulations to void coalescence is planned for future studies.

References

- [Bel02] J. Belak. How metals fail. *Lawrence Livermore National Laboratory, S&TR*, 7/8:317–327, 2002.
- [Fre98] L. B. Freund. *Dynamic Fracture Mechanics*. Cambridge University Press, 1998.
- [GS06] D. Gross and T. Seelig. *Bruchmechanik*. Springer, 2006.
- [MM00] S. Mercier and A. Molinari. Micromechanics of void growth at high rates. *Journal de Physique IV*, 10(P9):415–420, 2000.
- [MPE01] W. Muschik, C. Papenfuss, and H. Ehrentraut. A sketch of continuum thermodynamics. *Journal of Non-Newtonian Fluid Mechanics*, 96:255–290, 2001.
- [MPE04] W. Muschik, C. Papenfuss, and H. Ehrentraut. Mesoscopic theory of liquid crystals. *Journal of Non-Equilibrium Thermodynamics*, 29(1):75–106, 2004.
- [Mül01] Ingo Müller. *Grundzüge der Thermodynamik*. Springer Verlag, 2001.
- [OM92] M. Ortiz and A. Molinari. Effect of strain hardening and rate sensitivity on the dynamic growth of a void in a plastic material. *Transaction of the ASME*, 59:48–53, 1992.
- [RV02] L. Ratke and P.W. Voorhees. *Growth and Coarsening: Ostwald Ripening in Engineering Materials*. Springer, 2002.
- [SCA01] A. Strachan, T. Cagin, and Goddard W. A. Critical behavior in spallation failure of metals. *Physics Review B*, 63:060103, 2001.
- [TI77] K. Takagi and M. Ishii. Crystal growth of sapphire filaments by a laser-heated floating zone technique. *Journal of Materials Science*, 12, 1977.
- [Tve90] V. Tvergaard. Material failure by void growth to coalescence. *Advances in Applied Mechanics*, 27:83–151, 1990.
- [WB06] K. Weinberg and T. Böhme. Mesoscopic Modeling for Continua with Pores: Biological Soft Tissue. *submitted to: Non-Equilibrium Thermodynamics*, 2006.
- [Wei06] K. Weinberg. Material Models of Microstructured Solids — Theory, Numeric and Applications. Habilitationsschrift (eingereicht), TU Berlin, 2006.
- [WMO06] K. Weinberg, A. Mota, and M. Ortiz. A Variational Constitutive Model for Porous Metal Plasticity. *Computational Mechanics*, 37(2):142 – 152, 2006.
- [XP05] Luhua Xu and John H.L. Pang. Interfacial IMC and Kirkendall void on SAC solder joints subject to thermal cycling. *Proceedings of the 7th Electronics Packaging Technology Conference*, 2, 2005.



Recent Preprints in this Series

- 200 *A. Mielke, M. Ortiz*, A class of minimum principles for characterizing the trajectories and the relaxation of dissipative systems, 2006
- 201 *J. Giannoulis, M. Herrmann, A. Mielke*, Continuum descriptions for the dynamics in discrete lattices: derivation and justification, 2006
- 202 *J. W. Barrett, H. Garcke, R. Nürnberg*, On sharp interface limits of Allen–Cahn/Cahn–Hilliard variational inequalities, 2006
- 203 *K. Matthies*, Exponential Estimates in Averaging and Homogenisation, 2006
- 204 *H. Garcke, M. Lenz, B. Niethammer, M. Rumpf, U. Weikard*, Multiple Scales in Phase Separating Systems with Elastic Misfit, 2006
- 205 *H. Garcke, D. J. C. Kwak*, On asymptotic limits of Cahn–Hilliard systems with elastic misfit, 2006
- 206 *M. Kurzke, C. Melcher, R. Moser*, Domain walls and vortices in thin ferromagnetic films, 2006
- 207 *A. DeSimone, R.V. Kohn, S. Müller, F. Otto*, Recent analytical developments in micromagnetics, 2004
- 208 *S. Müller, M. G. Mora*, Derivation of a rod theory for multiphase materials, 2005
- 209 *A. Mielke, A. M. Timofte*, Two-scale homogenization for evolutionary variational inequalities via the energetic formulation, 2006
- 210 *A. Arnold, E. Dhamo, C. Manzini*, Dispersive effects in quantum kinetic equations, 2006
- 211 *T. Blesgen, I. Chenchiah*, A plasticity theory of solids undergoing phase transitions, 2006
- 212 *B. Stinner*, Weak solutions to a multi-phase field system of parabolic equations related to alloy solidification, 2007
- 213 *T. Böhme, K. Weinberg*, Mesoscopic modeling for continua with pores: applications to biological soft tissue, 2007
- 214 *T. Böhme, K. Weinberg*, Mesoscopic modeling for continua with pores: dynamic void growth in viscoplastic metals, 2007

To get these preprints, please visit

<http://www.mathematik.uni-stuttgart.de/~mehrskalen/>